ACS APPLIED MATERIALS & INTERFACES

Research Article

www.acsami.org

Self-Assembly of Gridlike Zinc Oxide Lamellae for Chemical-Sensing Applications

Jianping Du,*[,†] Ruihua Zhao,[‡] Shuai Chen,[∥] Heyan Wang,[†] Jinping Li,*[,§] and Zhenping Zhu[∥]

[†]College of Chemistry and Chemical Engineering, Taiyuan University of Technology, Taiyuan 030024, P. R. China

[‡]Shanxi Kunming Tobacco Limited Liability Company, Taiyuan 030012, Shanxi P. R. China

[§]Research Institute of Special Chemicals, Taiyuan University of Technology, Taiyuan 030024, P. R. China

[∥]Institute of Coal Chemistry, Chinese Academy of Science, Taiyuan 030001, P. R. China

Supporting Information

ABSTRACT: Hexagonal gridlike ZnO lamellae (GZL) with uniform thickness are synthesized by the *o*-phthalic acid-assisted hydrothermal method. Here, a systematic study of the assembly behaviors of gridlike ZnO lamellae obtained by the synergistic effect of urea and *o*-phthalic acid is presented. The morphology evolution and formation mechanism of GZL are also discussed in detail. The as-synthesized samples were characterized by powder X-ray diffraction, scanning electron microscopy, and transmission electron microscopy and electron diffraction spectroscopy. The results show that 2D ZnO lamellae are composed of nanotablets, which are jointed to form grids. The length and width of ZnO lamellae are about 1000 and 500 nm, respectively, and the thickness is about 30 nm. GZL morphology evolves from hexagonal ZnO nanotablets to lamellae with grids. The gas-sensing properties indicate that sensors fabricated from different materials present very different responses to volatile organic compounds. A GZL-based sensor has good response to acetaldehyde, and the response and recovery times are 1 and 6 s, respectively, when it was exposed to 1 ppm of acetaldehyde gas. The possibility of tuning the gas-sensing properties by adjusting the morphology makes GZL a novel candidate for more effective detection of a toxic, volatile gas with low concentration.

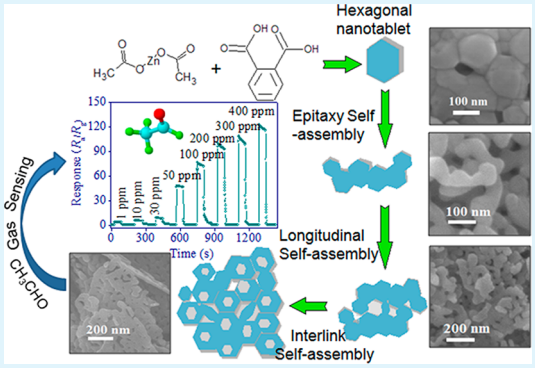

KEYWORDS: *zinc oxide, hexagonal nanotablet, self-assembly, morphology, sensing property*

1. INTRODUCTION

Nanomaterials, especially metal oxide semiconductors, play a key role in the future of many fields, including photocatalysis and sensing.[1,2] Among various metal oxide semiconductors, ZnO offers wide applications, such as use in optical probes,[3] photocatalysts,[4] solar cells,[5] biosensors,[6] light-emitting diodes,[7] and field-effect transistors.[8]

It is confirmed that zinc oxide, with wide band gap of 3.3 eV, is a promising candidate for use in fabricating sensors,[9] and the gas-sensing property of semiconductor materials is related closely to their morphologies and size.[10−12] Recently, chemical sensors fabricated from ZnO with different morphologies have been used to detect toxic gas and volatile organic compounds (VOCs), e.g., H_2S,[13] NO_2,[14] benzene,[15] ethanol,[16] and acetone.[17] Semiconductor ZnO films,[18] nanoparticles,[19] and nanorods[20] have also been prepared and used for detecting amines gas. Several works focused on detection of harmful acetaldehyde.[21,22] These VOCs easily cause environment health risks due to their extremely high volatility. Besides indoor sources, toxic VOCs vapors are released from burning of fossil fuels and oil, gas extraction, automobile exhaust, tobacco smoke, and the winemaking process. Acetaldehyde is also a product of ethanol oxidation.[21] Some toxic gases are released from outdoor sources under different temperatures conditions. So chemosensing detection of VOCs such as acetaldehyde is an important method. However, only limited research has focused on the detection of acetaldehyde using a ZnO-based sensor at high temperature.[21] On the basis of the detecting necessity, it is a challenge to develop novel sensing materials at different temperatures.

To improve the specific property of materials, different synthetic strategies proposed in the past few years focus on the controlling of shape and size.[23−26] It is well-known that surfactant-assisted methods easily achieve control of size and shape.[27−29] In spite of the existing routes, the synthesis of a ZnO 2D network-like nanomaterial that is surfactant/dopant-free is not widely available by simple, controllable self-assembly. Therefore, it is significant to assemble a 2D nanostructure without the use of surfactant for the soft-chemistry preparation and wide application.

Received: December 28, 2014
Accepted: February 24, 2015
Published: February 24, 2015

DOI: 10.1021/am509139f
ACS Appl. Mater. Interfaces 2015, 7, 5870−5878

Herein, we report a surfactant/dopant-free route to self-assemble 2D gridlike ZnO lamellae by combination of urea and *o*-phthalic acid. The morphological evolution mechanism of ZnO lamellae, composed of hexagonal tablets, and their sensing properties toward acetaldehyde and acetone were also investigated. The use of urea and/or *o*-phthalic acid can effectively control the morphological changes of ZnO at mild temperature, which is superior to the method of controlling morphology by changing temperature.[30] The excess amount of *o*-phthalic acid promotes growth of nanotablets toward the 2D swordlike ZnO. Optimizing the amount of *o*-phthalic acid can enhance production of hexagonal nanotablets. The synergistic effect of urea and *o*-phthalic acid makes the morphology evolve from nanotablets to 2D gridlike lamellae. Their sensitivity and selectivity to different VOCs have been obviously improved by their unique morphological features. Short response and recovery times demonstrate their potential application for fast-responding to low-concentration VOCs.

2. EXPERIMENTAL PROCEDURES

2.1. Synthesis of ZnO Nanomaterials. All chemical reagents used in the experimental are analytical grade without further purification. Nanosized ZnO with different morphologies was synthesized by an *o*-phthalic acid-assisted process followed by calcinations under air atmosphere. In a typical process, zinc acetate (6.6 g) and urea (3.6 g) were dissolved in deionized water (70 mL) with vigorous stirring, resulting in a transparent solution. *o*-Phthalic acid (1.5 g) was added into the above solution, and the mixture was mixed well by stirring for 30 min at room temperature. The mixed solution was then transferred into a Teflon-lined stainless steel autoclave. The autoclave was sealed and heated at 120 °C for 12 h and then it cooled to room temperature naturally. The product was collected by centrifugation, washed repeatedly with deionized water and absolute ethanol, and finally dried at 60 °C overnight. According to the above-described method, a series of samples was synthesized by changing the ratio of reactants and reaction time to explore the morphology evolution. After preparation, all ZnO nanomaterials were heat-treated at 500 °C for 2 h. The resulted powders were used for characterization and sensor preparation.

2.2. Characterization of ZnO Nanomaterials. The microstructure and morphologies of as-synthesized ZnO were observed by scanning electron microscopy (Hitachi S-4800, operated at 5 kV) and transmission electron microscopy (Hitachi H-800 with an accelerating voltage of 200 kV) equipped with EDX. The crystal structure of ZnO was investigated by X-ray diffraction (D/Max-2000 series, Cu Kα radiation, λ = 1.54 Å), from 2θ = 30° to 70°. The specific surface areas were analyzed by N_2 adsorption−desorption measurement, which was performed on a Micromeritics ASAP 2010 apparatus.

2.3. Fabrication of Sensors. A paste was prepared by mixing the as-synthesized ZnO with anhydrous ethanol. The obtained paste was coated onto an alumina ceramic tube with installed gold electrodes. After drying at 60 °C for 1 h in air, the ceramic tube was heated to 350 °C for 90 min in an electric furnace. A heater of Ni−Cr wire was inserted into the ceramic tube, which provided the working temperature of the gas sensor (Scheme 1). The gas-sensing properties of ZnO toward volatile organic compounds (VOCs) with various concentrations were studied by using a static test system (WS-30A, Winsen Electronics Co. Ltd., Henan Province, China). The target gas was injected into the testing chamber, using air as the diluting and reference gas. The sensing response of the sensor was defined as the ratio of the resistance in air (R_a) to that in a target gas (R_g). When the response reached a constant value, the sensor was taken out to recover in air. Each measure was performed three times to ensure reproducibility, and then the average response value was obtained.

Scheme 1. Schematic Illustration of Sensing Test[a]

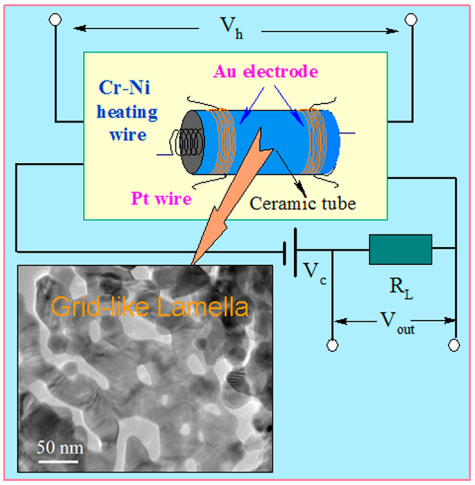

[a] V_c, circuit voltage; V_h, heating voltage; V_{out}, signal voltage; and R_L, load resistor.

3. RESULTS AND DISCUSSION

3.1. Self-Assembly of 2D Gridlike ZnO Lamellae (GZL). Representative SEM images reveal the morphology of the gridlike ZnO lamellae (GZL) in the presence of urea and *o*-phthalic acid. The ZnO powder consists of well-formed lamellae with small dense holes. The length of lamellae range from 0.5 to 1 μm (Figure 1a). Magnified SEM images show clear gridlike lamellae, and the length of a typical lamella is about 1 μm, which is labeled with a green arrow. The thickness of a single lamella is about 30 nm, as indicated by white arrows (Figure 1b). The side view shows that the gridlike ZnO lamellae are composed of nanoparticles with uniform size, and the average size is about 30 nm, as denoted with the black arrows, which is in agreement with the thickness of lamella observed from Figure 1b. These nanoparticles are linked together one by one, and the side face of each lamellae is just like a bead chain (Figure 1c).

The powder X-ray diffraction (XRD) spectrum of as-prepared GZL is presented in Figure 1d. The XRD pattern reveals that the gridlike ZnO lamellae has a high degree of crystallinity. All the diffraction peaks of GZL are well-indexed to the hexagonal wurtzite structure phase (JCPDS card no. 36-1451). Strong diffraction peaks are observed, appearing at the 2θ values of 31.91°, 34.29°, and 38.68°, which correspond to the (100), (002) and (101) planes.[17,18] The intensity of the peaks at 31.91° and 38.68° is higher than that of the peak at 34.29°, which may be a characteristic of GZL.

For further analysis, the TEM images of as-synthesized GZL provide insight into the structure of ZnO lamellae with grids. The monolayer grid structure of lamellae is observed clearly (Figure 2a). The HRTEM image shows that the net structures were formed by fusion and interconnection of a large number of nanoparticles (similar to nanotablets) (Figure 2b). The formed grids exhibit clear hexagon or deformed hexagon (marked with white lines). Hexagonal contours of some nanoparticles at the grid side are observed clearly, which are delineated by the white lines. A small nanoparticle is magnified and showed in Figure 2b. The longest diagonal length of hexagon is about 25 nm and the side length is about 12 nm (Figure 2b, inset). It is clear that the ZnO networks were formed by interconnection of hexagonal nanotablets in the

DOI: 10.1021/am509139f
ACS Appl. Mater. Interfaces 2015, 7, 5870−5878

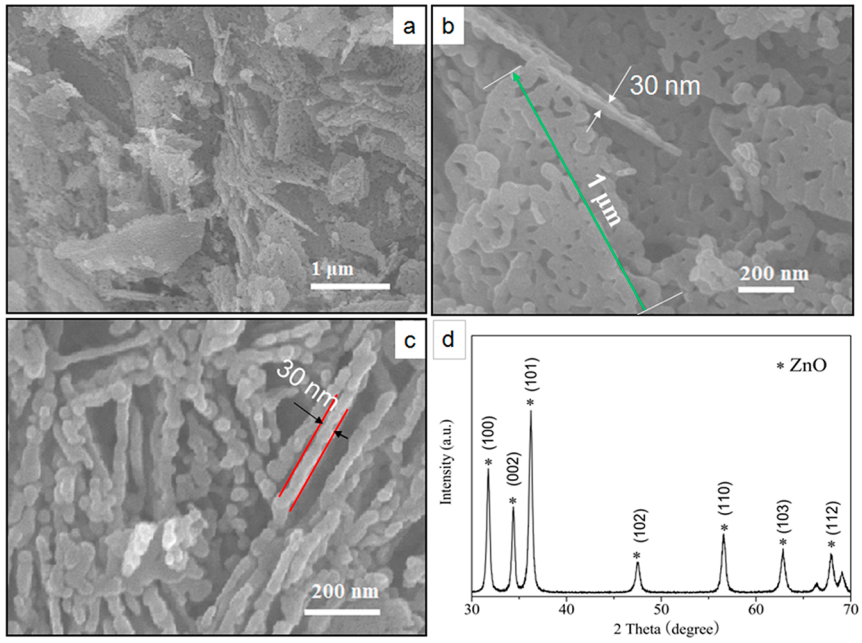

Figure 1. (a) SEM image of gridlike ZnO lamellae (GZL), prepared using zinc precursor, urea, and *o*-phthalic acid (mole ratio of 1:2:0.3). (b) Magnified SEM image of GZL. (c) SEM image of the side view of GZL. (d) XRD pattern of the as-assembled GZL sample.

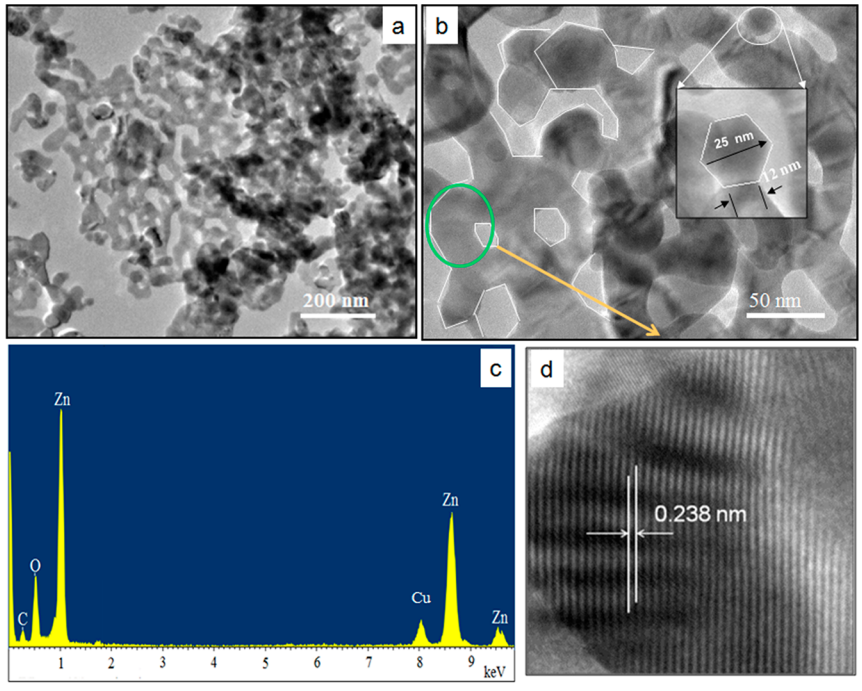

Figure 2. (a) TEM image of the as-assembled gridlike ZnO lamellae (GZL). (b) HRTEM image of the as-assembled GZL. The inset image shows a hexagonal nanotablet with perfect contour. (c) EDS spectrum that shows the components of GZL. (d) HRTEM image of the part of the GZL shown in part b.

presence of urea and *o*-phthalic acid. Figure 2c shows the EDS pattern of GZL powder. There are only zinc and oxygen peaks, besides the carbon and copper peaks that appear due to the carbon membrane in the Cu grid; this indicates that the GZL mainly consists of zinc and oxygen elements. A junction of net marked with the green oval (Figure 2b) was further magnified. The lattice fringes are well-organized in a proper manner, and no dislocation is found (Figure 2d). The lattice distance of the (100) plane of GZL along the longitudinal axis direction is about 0.238 nm, corresponding to the wurtzite hexagonal structures of ZnO, which is consistent with the XRD result (Figure 1d).

3.2. Morphology Evolution of 2D Gridlike ZnO Lamellae. The reaction of zinc acetate with urea yields ZnO fragments with small pores (Figure 3a). Fragmentary ZnO is self-assembled by interlinking of nanotablets, and the sizes are uniform (Figure 3b). The formed fragments with pores have not extended continually to form large lamellae. Self-assembly of the gridlike ZnO lamellae cannot be completed only using urea. A large number of ZnO nanoparticles were obtained by

DOI: 10.1021/am509139f
ACS Appl. Mater. Interfaces 2015, 7, 5870−5878

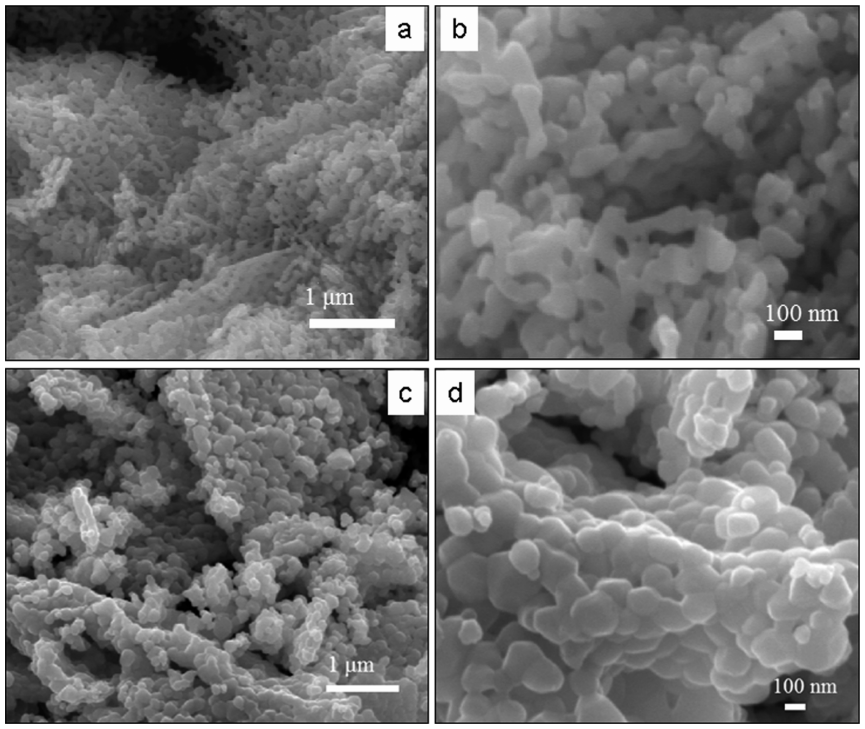

Figure 3. (a) SEM image of the fragmentary ZnO with fewer nets, prepared only using zinc precursor and urea (mole ratio of 1:2). (b) Magnified SEM image showing small fragments with fewer grids. (c) SEM image of the as-assembled ZnO nanoparticles without grid formation, prepared only using zinc precursor and *o*-phthalic acid (mole ratio of 1:0.3). (d) Magnified SEM image showing uniform hexagonal nanoparticles only being agglomerated to each other.

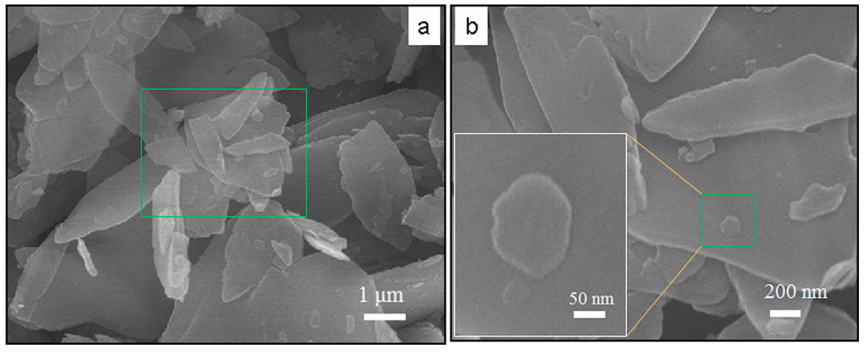

Figure 4. (a) SEM image of the nanometer ZnO fragments, prepared only using zinc precursor and *o*-phthalic acid (mole ratio of 1:3). (b) Magnified SEM image of ZnO, labeled with the green rectangle in part a. The inset image shows a hexagonal nanotablet, which is a magnification of the small particle on the slice labeled with a small, green square.

the reaction of zinc acetate with *o*-phthalic acid (Figure 3c). ZnO nanoparticles are well-dispersed and arranged in a monolayer. A magnified SEM image shows the uniform sizes ranging from 100 to 200 nm (Figure 3d). The Layer-ordered arrangement is observed clearly and no agglomerate is found. The as-synthesized ZnO nanoparticles exhibit a hexagonal shape in the presence of *o*-phthalic acid.

Increasing the amount of *o*-phthalic acid induced dramatic changes in the shape of as-synthesized ZnO. The morphologies of this sample are presented in Figure 4. Big lamellae with irregular morphology were formed, such as the strip- or slatlike ZnO shown. It is noted that each strip and slat has a triangle tip, which may be self-assembled by hexagonal ZnO nanoparticles (Figure 4a). After the rectangle area marked with the green frame was magnified, it is found that there are some small nanoparticles dispersed on the lamellar surface (Figure 4b). A single particle marked with a green square frame is further magnified. The perfect hexagonal nanotablet is observed clearly, and the size is about 100 nm (Figure 4b, inset). The strip- and slatlike ZnO with a triangle tip is more like a sword. The results evidenced the fact that the sword-shaped ZnO synthesized in the presence of excess *o*-phthalic acid is self-assembled by hexagonal ZnO nanotablets. The formation of nanosized ZnO experienced a fusion process of the hexagonal nanoparticles.

X-ray diffraction (XRD) patterns of these three samples prepared by adding urea and *o*-phthalic acid respectively are shown in Figure 5. The diffraction peaks of the as-synthesized ZnO are closely matched to the (100), (002), (101), (102), (110), (103), and (112) planes of the hexagonal wurtzite structure of ZnO (JCPDS card no. 36-1451). For the sample prepared only using urea, the intensity of the peak appearing at 34.29° is lower than the intensity of those at 31.91° and 38.68° (Figure 5a), which are similar to the characteristic peaks of GZL prepared in the presence of urea and *o*-phthalic acid

DOI: 10.1021/am509139f
ACS Appl. Mater. Interfaces 2015, 7, 5870−5878

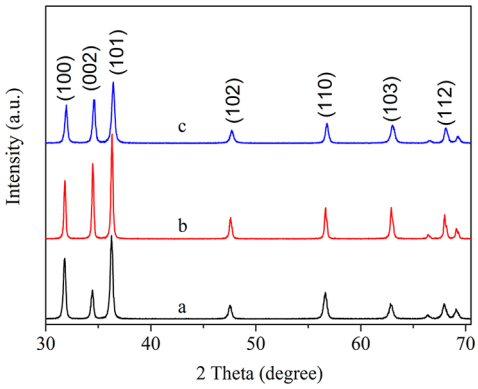

Figure 5. (a) X-ray diffraction (XRD) spectra of ZnO fragments with fewer grids, prepared only using zinc and precursor urea (mole ratio of 1:2). (b) XRD spectra of hexagonal ZnO nanotablets, prepared only using zinc precursor and *o*-phthalic acid (mole ratio of 1:0.3). (c) XRD spectra of the swordlike ZnO with few hexagonal nanotablets, prepared only using zinc precursor and *o*-phthalic acid (mole ratio of 1:3).

(Figure 1d). These may be a characteristic of gridlike ZnO lamella. For the samples prepared only using *o*-phthalic acid, the intensity of peaks increases with the values of 2θ increasing from 31.91° to 38.68° (Figure 5a,b). The perfect hexagonal ZnO nanoparticles exhibit the stronger intensity of peaks, suggesting a good crystalline structure.

3.3. Morphology Evolution and Formation Mechanism of 2D Gridlike ZnO Lamellae. To further investigate the morphology evolution, 2D GZL were synthesized by changing the growth time and molar ratio of starting materials, respectively. SEM and XRD measurements were performed (see Figures S1−S7 in the Supporting Information). After hydrothermal treatment at 120 °C for 3 h, the as-synthesized sample consists of nanoparticles, except with some nanorods (Figure 6). Selected areas marked with a green rectangle and square are magnified and displayed in parts b and c of Figure 6, respectively. From the high-resolution SEM image (Figure 6b), an almost uniform size and less agglomeration of nanotablets are observed clearly. It is found that nanotablets have outlined edges and corners, which is similar to a hexagonal shape. The W-type nanorods can also be found from the amplification of the green square area (Figure 6c). These nanorods, their length is about 300 nm, are self-assembled by several nanotablets and they may be the fragments of gridlike lamellae. The results indicate that the short-time hydrothermal treatment is enough to form ZnO nanotablets, but not enough to promote growth of fragments, which implies that elongating the reaction time would benefit the extension of fragments and self-assembly of lamellae. Further evidence has been provided by SEM measurement.

We synthesized the samples by using the same procedure and changing various hydrothermal treatment times. When hydrothermal treatment was maintained for 5 h at 120 °C, a gridlike or porous structure can be formed and the sample consists of a large amount of ZnO fragments (see Figure S1a in the Supporting Information). Nanoparticles and nanorods are not found in the sample. The HRTEM image shows that the W-type nanorods deform to form some ZnO fragments with grids, and some were closed incompletely (Figure S1b, Supporting Information), which tends to close each end and form the grids. The shape of the connection point is still similar to a nanotablet, suggesting that the ZnO fragment was self-

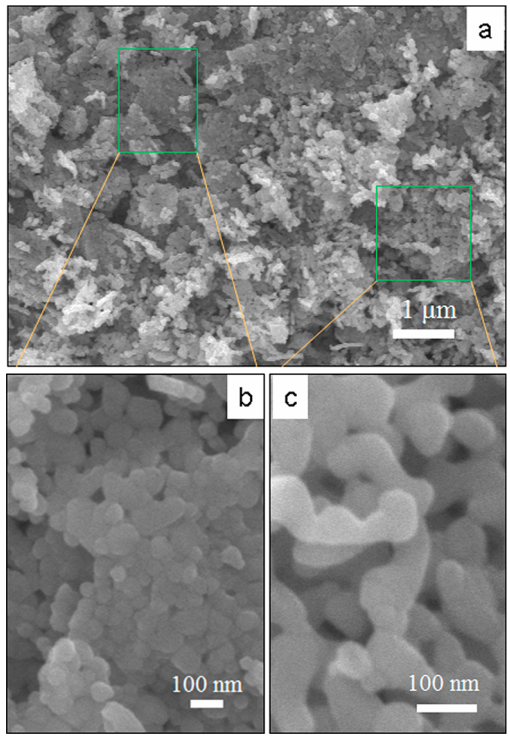

Figure 6. (a) SEM image of ZnO nanoparticles, prepared using zinc precursor, urea, and *o*-phthalic acid (mole ratio of 1:2:0.3) at 120 °C for 3 h. (b) Magnified SEM image of ZnO, labeled with a green rectangle in part a. (c) Magnified SEM image of ZnO, labeled with a green square in part a.

assembled by nanotablets along the epitaxy direction. After reaction for 8 h, the gridlike ZnO fragments have been formed (see Figure S2a in the Supporting Information). It is clear that the ends of curved ZnO nanorods have been closed and small fragments with grids were formed by self-assembly longitudinally (Figure S2b, Supporting Information). If the reaction time was elongated (up to 10 h) continuously, lamellar structures with grids are more obvious and extended lamellae are formed (see Figure S3a in the Supporting Information). The HRTEM image shows that the 2D gridlike ZnO lamellae are more intact and the fusion of interconnecting parts has been achieved (Figure S3b, Supporting Information). The formed grids exhibit hexagonal or deformed hexagonal pores, indicating that the formation of grids results from the fusion of hexagonal nanotablets. The XRD patterns of various ZnO samples are presented in Figure S4 (Supporting Information). A comparison of all XRD patterns reveals that the peak intensity of obtained nano-ZnO increases with longer reaction time. Other samples, which were obtained by the hydrothermal treatment for more than 8 h, have an obviously higher intensity than the others produced by a short reaction time. Moreover, the peak intensity changes further indicate an initial formation of gridlike ZnO fragments, which is in agreement with HRSEM observation.

Figure 7 shows morphologies of gridlike ZnO lamellae, synthesized by self-assembly of nanotablets after reaction for 14 h. A large amount of lamellae were formed (Figure 7a). From the surface of lamellae, large fusion areas and small grid pores are observed clearly (Figure 7b). Additional fragments and the W-type nanorods are also found. This can be explained by the competition effect of the growth and self-assembly of nanotablets, which play a key role in formation of gridlike

DOI: 10.1021/am509139f
ACS Appl. Mater. Interfaces 2015, 7, 5870−5878

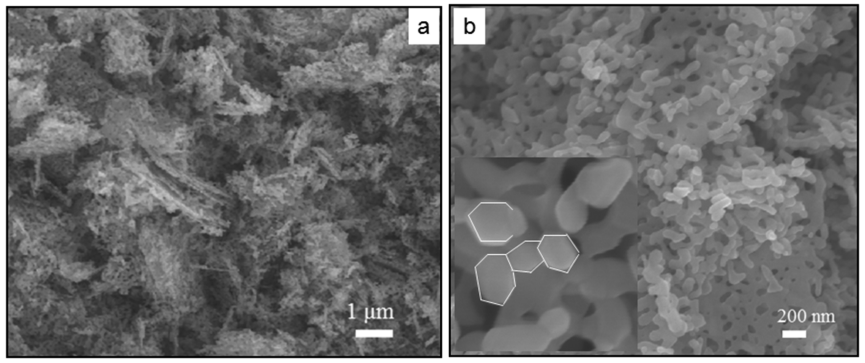

Figure 7. (a) SEM image of the gridlike ZnO lamellae, prepared using zinc precursor, urea, and *o*-phthalic acid (mole ratio of 1:2:0.3) at 120 °C for 14 h. (b) Magnified SEM image of ZnO. The inset image shows ZnO hexagonal nanotablets.

ZnO lamellae. Therefore, long hydrothermal times cause a high growth rate of nanotablets compared with their self-assembly. Hexagonal nanotablets marked with a white outline, i.e., building blocks of gridlike ZnO lamellae, were found clearly in the HRSEM image (Figure 7b, inset), which further supports the explanation.

Apart from the effect of the hydrothermal time, controlling the amount of *o*-phthalic acid induced dramatic changes to the shape of zinc oxide. When the molar ratio of zinc precursor and *o*-phthalic acid was up to 1, the gridlike ZnO lamellae decrease and more ZnO fragments appear (see Figure S5 in the Supporting Information). Especially, it is observed clearly that the gridlike ZnO lamellae were formed by interconnection of nanotablets, which exhibit clear hexagonal contours (Figure S5d, Supporting Information). When the molar ratio was decreased to 0.2, ZnO lamellae almost have not changed (see Figure S6 in the Supporting Information). If the selected area marked with a yellow rectangle is magnified, small fragments with imperfect grids are only found. In contrast, the intact extension of ZnO lamellae and hexagonal nanotablets has not been observed (Figure S6b, Supporting Information). This shows that an optimal amount of *o*-phthalic acid affects the formation of gridlike ZnO lamellae. XRD spectra indicate that the two samples have same hexagonal wurtzite structure (Figure S7, Supporting Information). However, the peak intensity of the (002) crystal plane is obviously different, which increases with the hexagonal nanotablet dominated ZnO transforming into the gridlike lamellae.

Herein, the self-assembly procedure of 2D gridlike ZnO lamellae is illustrated in Scheme 2. Zinc acetate was used as zinc source and *o*-phthalic acid as bridging ligand. The synergistic effect of urea and *o*-phthalic acid makes the morphology evolve from nanotablets to 2D gridlike lamellae. According to a similar template-directed mechanism,[31] hexagonal tabletlike nanoparticles were synthesized in the presence of *o*-phthalic acid, and then secondary self-assembly of hexagonal nanotablets as building block proceeded along the epitaxy direction, which led to the formation of W-shaped nanorods. A fragment with few grids was self-assembled by the interaction of strong oxygen−metal−oxygen bonds between nanorods along the longitudinal direction. Further self-assembly of fragments along different directions leads to formation of 2D lamellae. During a hydrothermal process, hexagonal pores of gridlike 2D lamellae were formed by interlinking hexagonal nanotablets, and they may also be generated by self-dissolution of the central part of hexagonal nanotablets. Subsequently, heat treatment of the amorphous lamellae with grids resulted in the formation of

Scheme 2. Morphology Evolution Mechanism for Self-Assembly of Gridlike ZnO Lamellae in the Presence of Urea and *o*-Phthalic Acid

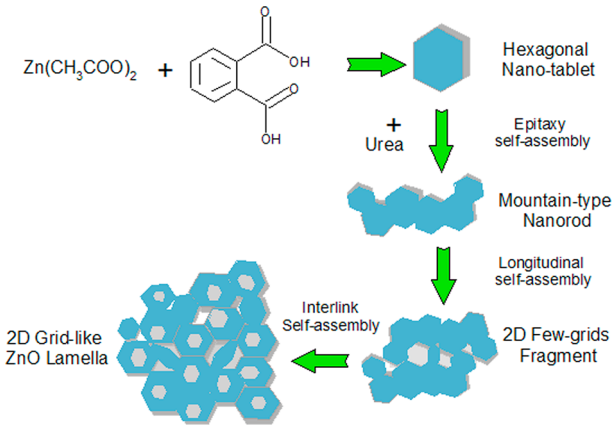

intact gridlike ZnO lamellae. The 2D gridlike lamellae structure is expected to provide an opportunity for applications such as solar cells, photocatalysts, chemical sensing, and biosensors.

3.4. Gas-Sensing Performance. In order to assess the gas-sensing properties of the as-synthesized ZnO, sensing tests of VOCs, including acetone, formaldehyde, acetaldehyde, methanol, ethanol, benzene, dimethylbenzene, and dichloromethane, have been carried out. Each experimental was done three times to reduce the error. Figure 8 shows the responses of the GZL to various VOCs gases at different temperatures. Sensor responses are strongly dependent on the operating temperature. We found that the responses to various gases increase with increasing temperature in the range from 160 to 300 °C, while the responses decrease above 300 °C. One possible reason is that more VOCs gas molecules can effectively react with the adsorbed oxygen ion on the surface of GZL with increasing temperature, which causes the increase in response.[32] If the temperature is higher than 300 °C, the adsorbed gas molecules desorbed rapidly and thus the chance of reaction decreased correspondingly, which results in the decrease in response. This agrees well with the reported results.[17,33] Therefore, the highest response of gridlike ZnO lamellae to VOCs gases, especially acetaldehyde, is found at 300 °C (Figure 8c). As the temperature goes up, ZnO with different morphologies, including ZnO fragments with few grids (see Figure S8 in the Supporting Information) and ZnO hexagonal nanotablets without nets (see Figure S9 in the Supporting Information), have the same trend in response change upon

DOI: 10.1021/am509139f
ACS Appl. Mater. Interfaces 2015, 7, 5870−5878

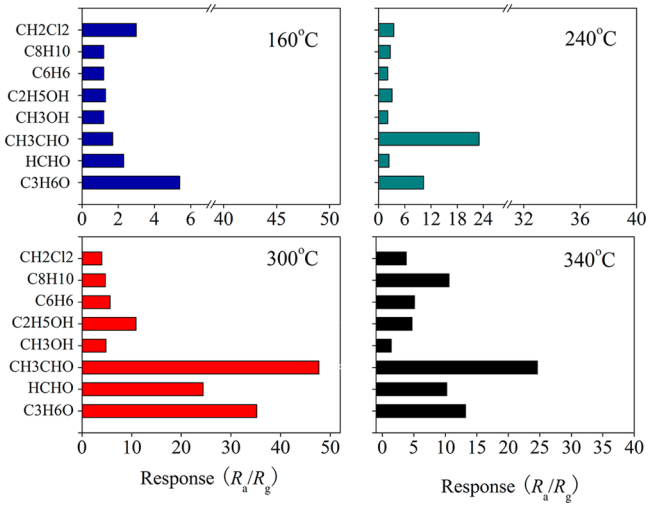

Figure 8. Gas responses of the as-assembled GZL sensor on exposure to 50 ppm of VOCs vapors at a temperature ranging from 160 to 340 °C [160 °C (blue bar), 240 °C (green bar), 300 °C (red bar), and 340 °C (black bar)].

exposure to 50 ppm of VOCs gases. For detecting acetaldehyde and acetone vapors, the optimal operating temperature is at 300 °C, which is lower than the reported value of 450 °C for acetaldehyde[21] and 420 °C for acetone.[17] This finding implies that as-synthesized ZnO has potential for application in detection of acetaldehyde and acetone. Additionally, the difference in gas-sensing properties is that ZnO with different morphologies exhibit different selectivities (Figures S8c and S9c, Supporting Information). Few-grid ZnO fragments have higher sensitivity to acetone compared with ZnO hexagonal nanotablets, while the sensitivity to ethanol for ZnO nanotablets is superior to that for the other two samples (GZL and ZnO fragments). Compared with commercialized ZnO powder, as-synthesized ZnO with controllable morphologies exhibits excellent sensing properties for detecting target VOCs at 300 °C (Figure S10, Supporting Information). This shows that the selectivity of ZnO for VOCs sensing can be controlled by the morphology transformation from hexagonal nanotablets to gridlike lamellae. Recently, a significant effort has been made to understand the influence of the morphology of zinc oxide nanostructures on its gas-sensing properties.[11,17,34] In addition, the specific surface areas of as-synthesized ZnO are about 18, 31, and 56 m^2/g for hexagonal nanotablets, few-grid fragments, and gridlike lamellae structures, respectively. Generally, different specific surface areas are related to the amount of absorbed oxygen. Thus, the electron depletion layer induced easily by oxygen adsorption on the surfaces has also a crucial effect on the gas-sensing properties.[35] Moreover, the sensing variation of different morphologies of ZnO can be explained by the distinctive structure and the species of adsorbed oxygen (O^{2-}, O^-, or O_2^-) on the surface of ZnO, which cause the change of

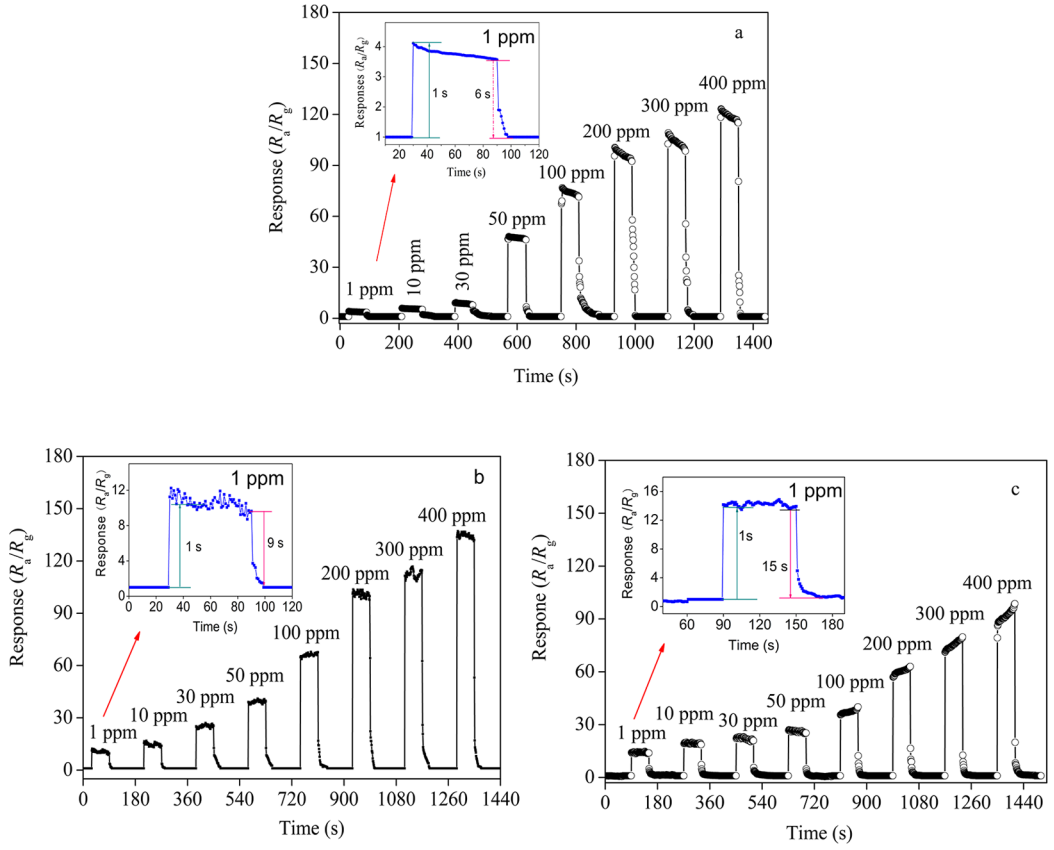

Figure 9. (a) Transient response of GZL-based sensor toward various concentrations (from 1 to 400 ppm) of acetaldehyde operated at 300 °C. The inset figure shows the response and recovery times of GZL on exposure to 1 ppm of acetaldehyde vapor. (b) Transient response of few-grid ZnO sensor toward various concentrations (from 1 to 400 ppm) of acetone operated at 300 °C. The inset figure shows the response and recovery times on exposure to 1 ppm of acetone vapor. (c) Transient response of hexagonal ZnO nanotablets sensor toward various concentrations (from 1 to 400 ppm) of acetone operated at 300 °C. The inset figure shows the response and recovery times on exposure to 1 ppm of acetone vapor.

DOI: 10.1021/am509139f
ACS Appl. Mater. Interfaces 2015, 7, 5870−5878

the depletion layer. The gridlike lamellae may favor the increase in oxygen adsorption to form oxygen adatoms and ions and may facilitate fast diffusion of the tested gas; thus, the reaction kinetic between the adsorbed oxygen species and gas molecules can be improved.

Gas response time and recovery time are very important to evaluate sensor performance. The transient response of a gridlike ZnO lamellae-based sensor toward acetaldehyde (1−400 ppm) is shown in Figure 9a. When the sensor was exposed to acetaldehyde gas (above 30 ppm), the response increased rapidly, while the response signal recovered quickly to the baseline when the sensor was disengaged from the tested circumstance. It is also found that the GZL sensor has low stability when it was exposed to 200−400 ppm acetaldehyde. The possible reason is that reactant molecules cannot react immediately with the limited adsorbed oxygen ions as the concentration of target gas increases; thus, gas molecules may escape before the reaction due to competitive adsorption and chemical activation.[32,33] The inset image emphasizes the response and recovery characteristics upon exposure to 1 ppm acetaldehyde. The response time and recovery time were about 1 and 6 s, respectively, suggesting that the gridlike ZnO lamellae structure is effective to capture low-concentration acetaldehyde molecules and to desorb them rapidly through the extended gridlike lamellae structure.

Both few-grid ZnO fragments and hexagonal nanotablets exhibit rapid response and recovery upon exposure to 1−400 ppm of acetone gas (Figure 9b,c). Especially when the concentrations are less than 50 ppm, the sensors have obvious responses to acetone. In the range of 1−400 ppm, ZnO sensors based on few-grid fragment and hexagonal nanotablet structures have a higher response to acetone than the reported ZnO nanosheet and nanoparticle sensor,[17] and they are also superior to the modified nanospheres.[34] The sensors based on few-grid ZnO fragments remain relatively stable in their response time, while the sensors based on hexagonal ZnO nanotablets exhibit an increase in the response to acetone from 100 to 400 ppm, which may be caused by different chemisorbed oxygen species for ZnO with different morphologies.[35] The response time was about 1 s, while the recovery time was 9 and 15 s, respectively, for the sensors based on few-grid fragments and hexagonal nanotablets (Figure 9b,c, inset). This shows that the adsorbed oxygen ions on the surface of nanotablets provide strong adsorption reaction sites, which result in slow desorption of target gas molecules. For the different mophologies of ZnO, the sensing difference may contribute to the receptor function and impact the surfaces utilized for the sensing material.

4. CONCLUSION

In summary, 2D gridlike ZnO lamellae self-assembled by hexagonal nanotablets were synthesized by an *o*-phthalic acid-assisted method. The morphology evolved from self-assembled hexagonal nanotablets and fragments with few nets to extended 2D lamellae with grids. Optimizing the amount of *o*-phthalic acid benefits the growth of hexagonal nanotablets and enhances the self-assembly behavior of fragments and gridlike ZnO lamellae. Zinc oxide with different morphologies are proved to have different selectivities and short response−recovery time for VOCs gases due to the accessible surface and extended grid structures. This tunability of morphology-dependent gas sensing is important to aid the development of a general method for fabrication of novel sensing materials. In the case of morphology-evolved ZnO, the gas-sensing properties of the sensors make them a candidate for detection of target VOC gases with low concentration. More works are underway in our laboratory to use the grid-lamellae ZnO semiconductor for photocatalytic and related optical applications.

■ ASSOCIATED CONTENT

Supporting Information

X-ray diffraction (XRD), scanning electron microscopy (SEM), and sensing properties of ZnO with different morphologies. This material is available free of charge via the Internet at http://pubs.acs.org.

■ AUTHOR INFORMATION

Corresponding Authors

*J.D. e-mail: dujp518@163.com.
*J.L. e-mail: jpli211@hotmail.com.

Notes

The authors declare no competing financial interest.

■ ACKNOWLEDGMENTS

The authors thank partial financial support by National Natural Science Foundation of China (21136007) and Natural Science Foundation of Shanxi Province (2014011016-4).

■ REFERENCES

(1) Heiligtag, F. J.; Cheng, W.; Mendonça, de V. R.; Süess, M. J.; Hametner, K.; Günther, D.; Ribeiro, C.; Niederberger, M. Self-Assembly of Metal and Metal Oxide Nanoparticles and Nanowires into a Macroscopic Ternary Aerogel Monolith with Tailored Photocatalytic Properties. *Chem. Mater.* **2014**, *26*, 5576−5584.

(2) Asefa, T.; Duncanc, C. T.; Sharma, K. K. Recent Advances in Nanostructured Chemosensors and Biosensors. *Analyst* **2009**, *134*, 1980−1990.

(3) Shinde, S. L.; Nanda, K. K. Wide-Range Temperature Sensing using Highly Sensitive Green-Luminescent ZnO and PMMA-ZnO Film as a Non-Contact Optical Probe. *Angew. Chem.* **2013**, *125*, 11535−11538.

(4) Qin, H. C.; Li, W. Y.; Xia, Y. J.; He, T. Photocatalytic Activity of Heterostructures Based on ZnO and N-Doped ZnO. *ACS Appl. Mater. Interfaces* **2011**, *3*, 3152−3156.

(5) Xu, J.; Chen, Z. H.; Zapien, J. A.; Lee, C. S.; Zhang, W. J. Surface Engineering of ZnO Nanostructures for Semiconductor-Sensitized Solar Cells. *Adv. Mater.* **2014**, *26*, 5337−5367.

(6) Yang, K.; She, G. W.; Wang, H.; Ou, X. M.; Zhang, X. H.; Lee, C. S.; Lee, S. T. ZnO Nanotube Arrays as Biosensors for Glucose. *J. Phys. Chem. C* **2009**, *113*, 20169−20172.

(7) Lupan, O.; Pauporte, T.; Le Bahers, T.; Viana, B.; Ciofini, I. Wavelength-Emission Tuning of ZnO Nanowire-Based Light-Emitting Diodes by Cu Doping: Experimental and Computational Insights. *Adv. Funct. Mater.* **2011**, *21*, 3564−3572.

(8) Frenzel, H.; Lajn, A.; von Wenckstern, H.; Lorenz, M.; Schein, F.; Zhang, Z. P.; Grundmann, M. Recent Progress on ZnO-Based Metal-Semiconductor Field-Effect Transistors and Their Application in Transparent Integrated Circuits. *Adv. Mater.* **2010**, *22*, 5332−5349.

(9) Menzel, A.; Subannajui, K.; Güder, F.; Moser, D.; Paul, O.; Zacharias, M. Multifunctional ZnO-Nanowire-Based Sensor. *Adv. Funct. Mater.* **2011**, *21*, 4342−4348.

(10) Li, Z. P.; Pan, W. X.; Zhang, D. J.; Zhan, J. H. Morphology-Dependent Gas-Sensing Properties of ZnO Nanostructures for Chlorophenol. *Chem.− Asian J.* **2010**, *5*, 1854−1859.

(11) Rai, P.; Kwak, W. K.; Yu, Y. T. Solvothermal Synthesis of ZnO Nanostructures and Their Morphology-Dependent Gas-Sensing Properties. *ACS Appl. Mater. Interfaces* **2013**, *5*, 3026−3032.

(12) Khan, A. A.; Khalid, M. Synthesis of Nano-Sized ZnO and Polyaniline-Zinc Oxide Composite: Characterization, Stability in

DOI: 10.1021/am509139f
ACS Appl. Mater. Interfaces 2015, 7, 5870−5878

Terms of dc Electrical Conductivity Retention and Application in Ammonia Vapor Detection. *J. Appl. Polym. Sci.* **2010**, *117*, 1601−1607.
(13) Iversen, K. J.; Spencer, M. J. S. Effect of ZnO Nanostructure Morphology on the Sensing of H_2S Gas. *J. Phys. Chem. C* **2013**, *117*, 26106−26108.
(14) Bai, S. L.; Chen, L. Y.; Hu, J. W.; Li, D. Q.; Luo, R. X.; Chen, A. F.; Liu, C. C. Synthesis of Quantum Size ZnO Crystals and Their Gas Sensing Properties for NO_2. *Sens. Actuators, B* **2011**, *159*, 97−102.
(15) Yao, M. S.; Hu, P.; Cao, Y. B.; Xiang, W. C.; Zhang, X.; Yuan, F. L.; Chen, Y. F. Morphology-Controlled ZnO Spherical Nanobelt-Flower Arrays and Their Sensing Properties. *Sens. Actuators, B* **2013**, *177*, 562−569.
(16) Tian, Y.; Li, J. C.; Xiong, H.; Dai, J. G. Controlled Synthesis of ZnO Hollow Microspheres Via Precursor-Template Method and Its Gas Sensing Property. *Appl. Surf. Sci.* **2012**, *258*, 8431−8438.
(17) Xiao, Y. H.; Lu, L. Z.; Zhang, A. Q.; Zhang, Y. H.; Sun, L.; Huo, L.; Li, F. Highly Enhanced Acetone Sensing Performances of Porous and Single Crystalline ZnO Nanosheets: High Percentage of Exposed (100) Facets Working Together with Surface Modification with Pd Nanoparticles. *ACS Appl. Mater. Interfaces* **2012**, *4*, 3797−3804.
(18) Roy, S.; Basu, S. ZnO Thin Film Sensors for Detecting Dimethyl- and Trimethylamine Vapors. *J. Mater. Sci. Mater. Electron.* **2004**, *15*, 321−326.
(19) Tang, H. X.; Yan, M.; Ma, X. F.; Zhang, H.; Wang, M.; Yang, D. R. Gas Sensing Behavior of Polyvinylpyrrolidone-Modified ZnO Nanoparticles for Trimethylamine. *Sens. Actuators B* **2006**, *113*, 324−328.
(20) Ameen, S.; Akhtar, M. S.; Shin, H. S. Low Temperature Grown ZnO Nanotubes as Smart Sensing Electrode for the Effective Detection of Ethanolamine Chemical. *Mater. Lett.* **2013**, *106*, 254−258.
(21) Gibertia, A.; Carotta, M. C.; Fabbri, B.; Gherardi, S.; Guidi, V.; Malagù, C. High-Sensitivity Detection of Acetaldehyde. *Sens. Actuators, B* **2012**, *174*, 402−405.
(22) Bastakoti, B. P.; Torad, N. L.; Yamauchi, Y. Polymeric Micelle Assembly for the Direct Synthesis of Platinum-Decorated Mesoporous TiO_2 toward Highly Selective Sensing of Acetaldehyde. *ACS Appl. Mater. Interfaces* **2014**, *6*, 854−860.
(23) Rai, P.; Khan, R.; Ahmad, R.; Hahn, Y. B.; Lee, I. H.; Yu, Y. T. Gas Sensing Properties of Single Crystalline ZnO Nanowires Grown by Thermal Evaporation Technique. *Curr. Appl. Phys.* **2013**, *13*, 1769−1773.
(24) Devan, R. S.; Patil, R. A.; Lin, J. H.; Ma, Y. R. One-Dimensional Metal-Oxide Nanostructures: Recent Developments in Synthesis, Characterization, and Applications. *Adv. Funct. Mater.* **2012**, *22*, 3326−3370.
(25) Ghashghaie, S.; Marzbanrad, E.; Raissi, B.; Zamani, C.; Riahifar, R. Effect of Low Frequency Electric Field Parameters on Chain Formation of ZnO Nanoparticles for Gas Sensing Applications. *J. Am. Ceram. Soc.* **2012**, *95*, 1843−1850.
(26) Gedamu, D.; Paulowicz, I.; Kaps, S.; Lupan, O.; Wille, S.; Haidarschin, G.; Mishra, Y. K.; Adelung, R. Rapid Fabrication Technique For Interpenetrated ZnO Nanotetrapod Networks for Fast UV Sensors. *Adv. Mater.* **2014**, *26*, 1541−1550.
(27) Tang, H.; Chang, J. C.; Shan, Y. Y.; Lee, S. T. Surfactant-Assisted Alignment of ZnO Nanocrystals to Superstructures. *J. Phys. Chem. B* **2008**, *112*, 4016−4021.
(28) Du, J. P.; Wang, H. Y.; Zhao, R. H.; Xie, Y. J.; Yao, H. L. Surfactant-Assisted Synthesis of the Pencil-like Zinc Oxide and Its Sensing Properties. *Mater. Lett.* **2013**, *107*, 259−261.
(29) Du, J. P.; Yao, H. L.; Zhao, R. H.; Wang, H. Y.; Xie, Y. J.; Li, J. P. Controllable Synthesis of Prism- and Lamella-like ZnO and Their Gas Sensing. *Mater. Lett.* **2014**, *136*, 427−430.
(30) Hu, Y.; Mei, T.; Guo, J.; White, T. Temperature-Triggered Self-Assembly of ZnO: From Nanocrystals to Nanorods to Tablets. *Inorg. Chem.* **2007**, *46*, 11031−11305.
(31) Jung, S.; Cho, W.; Lee, H. J.; Oh, M. Self-Template-Directed Formation of Coordination-Polymer Hexagonal Tubes and Rings, and Their Calcination to ZnO Rings. *Angew. Chem.* **2009**, *121*, 1487−1490; *Angew. Chem., Int. Ed.* **2009**, *48*, 1459−1462.
(32) Herran, J.; Fernández-González, O.; Castro-Hurtado, I.; Romero, T.; Mandayo, G. G.; Castăno, E. Photoactivated Solid-State Gas Sensor for Carbon Dioxide Detection at Room Temperature. *Sens. Actuators, B* **2010**, *149*, 368−372.
(33) Alenezi, M. R.; Alshammari, A. S.; Jayawardena, K. D. G. I.; Beliatis, M. J.; Henley, S. J.; Silva, S. R. P. Role of the Exposed Polar Facets in the Performance of Thermally and UV Activated ZnO Nanostructured Gas Sensors. *J. Phys. Chem. C* **2013**, *117*, 17850−17858.
(34) Li, X. W.; Zhou, X.; Guo, H.; Wang, C.; Liu, J. Y.; Sun, P.; Liu, F. M.; Lu, G. Y. Design of Au@ZnO Yolk−Shell Nanospheres with Enhanced Gas Sensing Properties. *ACS Appl. Mater. Interfaces* **2014**, *6*, 18661−18667.
(35) Yamazoe, N.; Sakai, G.; Shimanoe, K. Oxide Semiconductor Gas Sensors. *Catal. Surv. Asia* **2003**, *7*, 63−75.

DOI: 10.1021/am509139f
ACS Appl. Mater. Interfaces 2015, 7, 5870−5878